EurJOC European Journal of Organic Chemistry

FULL PAPER

DOI: 10.1002/ejoc.201500160

Remote Substituent Effects on the Stereoselectivity and Organocatalytic Activity of Densely Substituted Unnatural Proline Esters in Aldol Reactions

María de Gracia Retamosa,[a] Abel de Cózar,[a,b] Mirian Sánchez,[a] José I. Miranda,[c] José M. Sansano,[d] Luis M. Castelló,[d] Carmen Nájera,[d] Ana I. Jiménez,[e] Francisco J. Sayago,[e] Carlos Cativiela,[e] and Fernando P. Cossío*[a]

Keywords: Organocatalysis / Aldol reactions / Kinetics / Reaction mechanisms / Transition states

The organocatalytic activities of highly substituted proline esters obtained through asymmetric [3+2] cycloadditions of azomethine ylides derived from glycine iminoesters have been analyzed by ^{19}F NMR and through kinetic isotope effects. Kinetic rate constants have been determined for unnatural proline esters incorporating different substituents. It has been found that *exo*-L and *endo*-L unnatural proline methyl esters yield opposite enantiomers in aldol reactions between cyclic ketones and aromatic aldehydes. The combined results reported in this study show subtle and remote effects that determine the organocatalytic behavior of these synthetic but readily available amino acid derivatives. These data can be used as design criteria for the development of new pyrrolidine-based organocatalysts.

Introduction

The aldol reaction is one of the most important reactions for the convergent generation of C–C bonds.[1] This transformation is operative in biochemical processes, type I and II aldolases being the main representative enzymes.[2] Although it has been known since 1971–1974 that L-proline (L-Pro) can catalyze intramolecular aldol reactions,[3,4] the 2000 report by Barbas and List[5,6] of intermolecular aldol reactions catalyzed by L-Pro prompted an impressive upsurge of work on this reaction.[7] The term organocatalysis, explicitly mentioned by MacMillan[8] in a paper also published in 2000, contributed to placing these reactions in a well-defined and readily identifiable category. Thus, different organocatalysts have been tested in aldol reactions;[9] they include natural amino acids[10] such as histidine,[11] serine,[12] threonine,[12,13] tryptophan,[12,14] alanine,[15] and isoleucine.[16] Of these natural amino acids, L-Pro (and its derivatives) has emerged as the most widely used organocatalysts for the aldol reaction. Trost and Brindle,[17] in their comprehensive review published in 2010, reported around 45 L-Pro derivatives that are able to catalyze aldol reactions. It is relevant to note that in all these cases the stereochemistry of the major aldol adducts was found to be the same: namely, that associated with the (2*S*,1′*R*) configuration in the new chiral carbon atoms (Scheme 1).

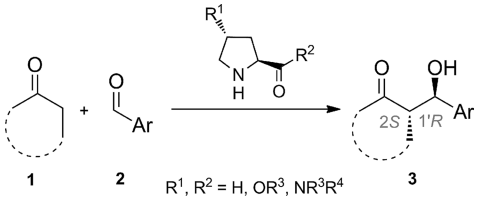

Scheme 1. Stereochemical outcome observed in aldol reactions catalyzed by L-Pro derivatives.

The mechanism and origin of the stereocontrol of L-Pro-catalyzed aldol reactions have been studied both experimentally[18] and computationally.[19] The generally accepted mechanism is shown in Figure 1. According to this catalytic cycle, the first stage of the reaction involves the formation of enamine intermediates of type **INT1**, a process that can be promoted by acidic protons present in the starting amino acid or in the reaction medium.[20] These intermediates have

[a] Departamento de Química Orgánica I / Kimika Organikoa I Saila, and Centro de Innovación en Quíimica Avanzada (ORFEO-CINQA), Facultad de Química / Kimika Fakultatea, Universidad del País Vasco / Euskal Herriko Unibertsitatea (UPV/EHU), and Donostia International Physics Center (DIPC),
P. K. 1072, 20018 San Sebastián - Donostia, Spain
E-mail: fp.cossio@ehu.es
http://www.ehu.eus/eu/web/qbmm/hasiera
[b] IKERBASQUE, Basque Foundation for Science, 48013 Bilbao, Spain
[c] SGIker NMR Facility, 20018 San Sebastián - Donostia, Spain
[d] Departamento de Química Orgánica e Instituto de Síntesis Orgánica (ISO), and Centro de Innovación en Química Avanzada (ORFEO-CINQA). Facultad de Ciencias, Universidad de Alicante, 03080 Alicante, Spain
[e] Departamento de Química Orgánica, Instituto de Síntesis Química y Catálisis Homogénea (ISQCH), CSIC-Universidad de Zaragoza, 50009 Zaragoza, Spain

Supporting information for this article is available on the WWW under http://dx.doi.org/10.1002/ejoc.201500160.

been characterized spectroscopically[21] and by X-ray diffraction analysis.[22]

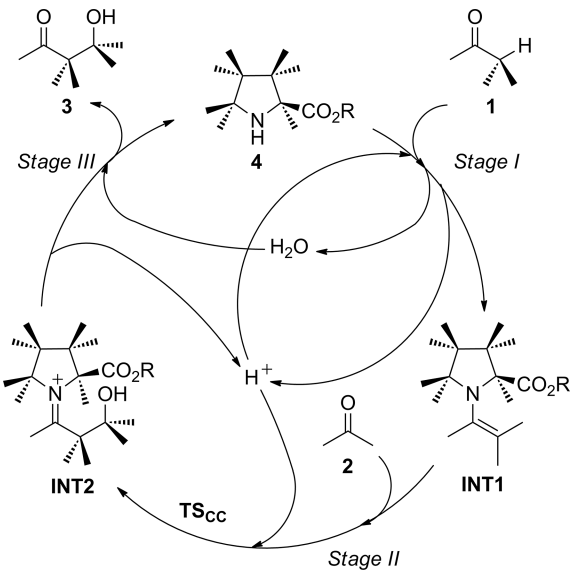

Figure 1. General catalytic cycle of aldol reactions catalyzed by L-proline derivatives. Unless otherwise indicated, the possible substituents at the different positions have not been specified.

Formation of the new C–C bond takes place during the second stage of the reaction (Figure 1), giving rise to iminium intermediates of type **INT2**. Once again, when L-Pro is used, the carboxy group provides the proton required to enhance the electrophilicity of a carbonyl compound **2**. The overall arrangement of the transition structures of type **TScc** associated with this stage, usually referred to as the Houk–List model,[23] shows a chair-like shape in which the Zimmerman–Traxler[24] arrangement is extended to form a cyclic transition structure involving the carboxy group of the organocatalyst. Finally, the iminium intermediate of type **INT2** is hydrolyzed to release the aldol **3** and the organocatalyst **4**, thus completing the catalytic cycle (Figure 1). It is important to note, however, that the Houk–List model relies on the presence of an acidic residue in the organocatalyst. When other functional groups such as ester, amido, amino, etc.[7b,7g] ■■ ((<=Author: change ref 7f–>7g correct??)) ■■ are present instead of the carboxylic acid, acidic additives or protic substituents are usually required. Although the origins of stereocontrol in these cases are far from being fully understood, computational studies on selected systems[19a] have shown that transition structures closely related to the Houk–List model are compatible with the observed stereochemical outcomes.

According to this conceptual framework, the stereochemistry of the reaction is determined by the L configuration of the amino acid and the distal (*anti*) conformation of the enamine double bond with respect to the carboxy group.[23] Therefore, it is not surprising that L-Pro derivatives yield the same enantiomers in reactions of this kind.

To the best of our knowledge, no structure–activity relationship studies on the organocatalytic properties of synthetic densely substituted L-proline derivatives have been reported to date. These compounds show great promise in the field and are easily accessible because the 2-alkoxycarbonylpyrrolidine scaffold can be formed in a single step through [3+2] cycloaddition between readily available π-deficient alkenes and azomethine ylides generated in situ.[25] Recently, we have reported new ferrocenyl-containing proline catalysts that are able to yield both *endo*- and *exo*-L-4-nitroproline esters with high enantiocontrol.[26] We also showed that the *exo* cycloadducts are able to catalyze the aldol reaction efficiently.[26] Here we compare the performances of L-4-nitroproline esters and acids featuring different substitution patterns and stereochemical configurations as organocatalysts in the aldol reaction. The ultimate goal of this research is to provide design criteria for organocatalysts based on unnatural proline esters obtained directly through fully stereocontrolled [3+2] cycloadditions.

Results and Discussion

Preparation of Unnatural Proline Organocatalysts

We prepared different L-4-nitroproline esters through asymmetric 1,3-dipolar cycloaddition reactions between different dipolarophiles and azomethine ylides formed in situ from the corresponding imines (Scheme 2 and Scheme 3). The reactions were catalyzed by enantiopure 5-ferrocenyl-4-nitroprolines L-**5a** and D-**5b** or phosphoramidite (S_a-*R*,*R*)-**6**, previously developed and tested as catalysts for reactions of this type by the San Sebastián-Donostia[26] and Alicante[27] groups, respectively (Scheme 2).

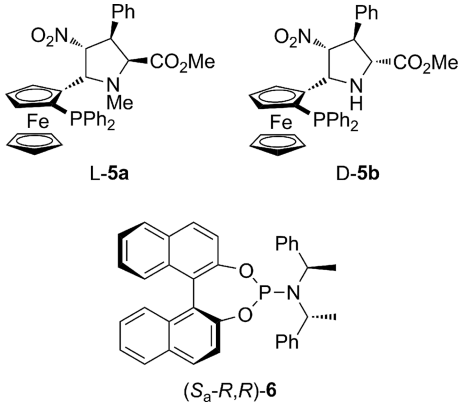

Scheme 2. Catalysts used in the synthesis of unnatural L-prolines **4**.

By use of glycine iminoesters **7a**–**f** as precursors of azomethine ylides, nitroalkenes **8a**–**c** as dipolarophiles, and L-**5a**, D-**5b**, or (S_a-*R*,*R*)-**6** as catalysts, *endo*- and *exo*-L-**4**-nitro-

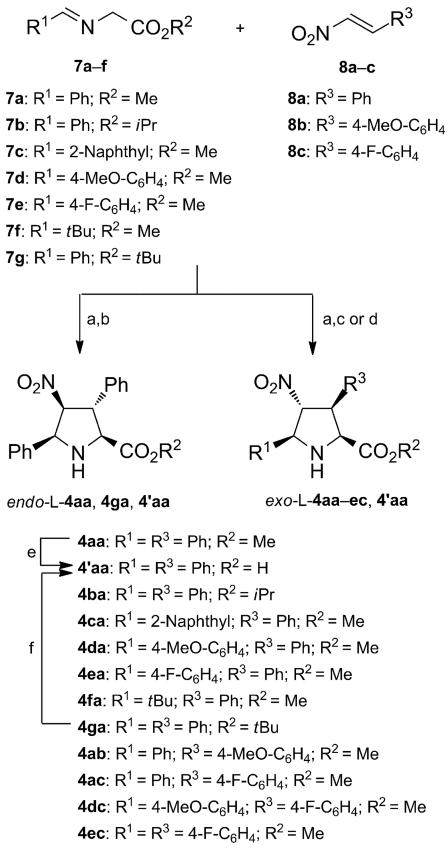

Scheme 3. Synthesis of unnatural L-proline derivatives *endo*-L-**4aa** and *exo*-L-**4aa**–**ec**. Reagents and conditions: (a) $Cu(CH_3CN)_4PF_6$ (3 mol-%), NEt_3 (5 mol-%), THF; (b) L-**5a** (3 mol-%), –60 °C; (c) D-**5b** (3 mol-%), –20 °C; (d) $Cu(OTf)_2$, (5 mol-%), (S_a-*R*,*R*)-**6** (5 mol-%), NEt_3 (5 mol-%), toluene, r.t. (e) NaOH, H_2O/acetone, r.t. (f) TFA, CH_2Cl_2, r.t.

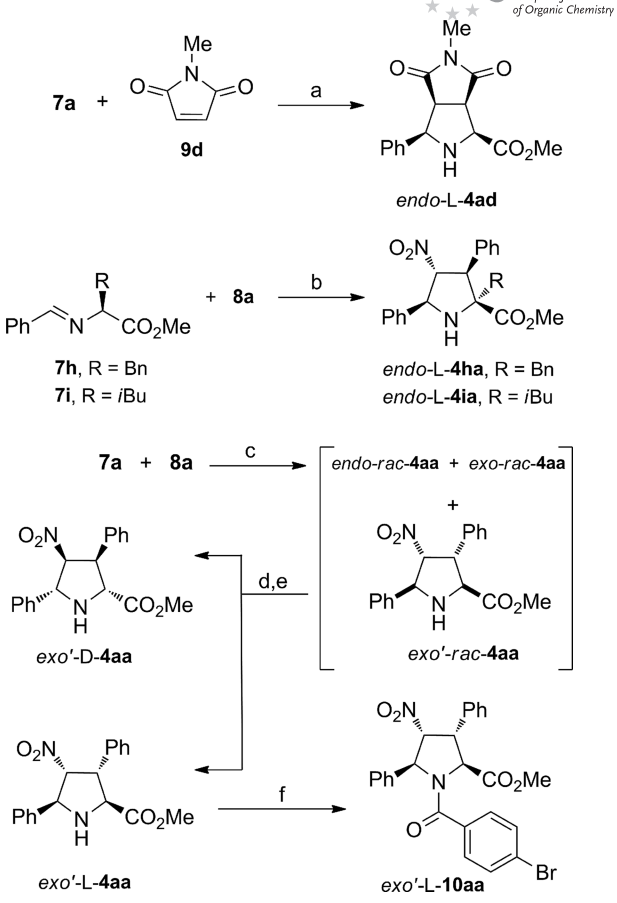

Scheme 4. Synthesis of unnatural L-proline esters *endo*-L-**4ad**, *exo*-L-**4ha**, *exo*-L-**4ia**, and *exo'*-L-**4aa**. Reagents and conditions: (a) $Cu(CH_3CN)_4PF_6$ (3 mol-%), D-**5b** (3 mol-%), NEt_3 (3 mol-%), THF, r.t.; (b) $Cu(OTf)_2$, (5 mol-%), (S_a-*R*,*R*)-**6** (5 mol-%), NEt_3 (5 mol-%), toluene, r.t.; (c) AgOAc (15 mol-%), NEt_3 (15 mol-%), CH_3CN, r.t.; (d) column chromatography on silica gel to isolate *exo'*-*rac*-**4aa**; (e) preparative HPLC resolution on a chiral column (Chiralpak® IB); (f) 4-bromobenzoyl chloride (2.0 equiv.), DIPEA (2.6 equiv.), $CHCl_3$, r.t.

proline esters **4aa**–**ec** were obtained (Scheme 3). In all cases, good yields and high optical purities were achieved.[26] When R^1 was a secondary alkyl group, such as cyclohexyl, the desired cycloadducts were not formed. However, in the case of R^1 = *tert*-butyl, *exo*-L-**4fa** was obtained with high enantiomeric excess. When *N*-methylmaleimide (**9d**) was used as the dipolarophile in the presence of D-**5b** as a catalyst, *endo*-L-**4ad** was isolated (Scheme 4). Unfortunately, imine **7h**, derived from L-phenylalanine methyl ester, gave poor enantiomeric excesses in the presence of either L-**5a** or D-**5b**. However, a catalytic amount of phosphoramidite (S_a-*R*,*R*)-**6** promoted the formation of *exo*-L-**4ha** as the sole enantiomer (Scheme 4).[27] This catalyst was also effective in the preparation of *exo*-L-**4ia** from imine **7i**. Therefore, our previously reported methodologies,[26,27] provided a convenient route to cycloadducts *endo*- and *exo*-L-**4aa**–**ga** as enantiopure compounds in high yields from easily or commercially available reactants (**7**,[28] **8**, and **9**) in the presence of readily accessible catalysts (Scheme 2). Such cycloadducts were isolated in useful quantities for subsequent evaluation as organocatalysts.

With the aim of further increasing the stereochemical diversity of the L-4-nitroproline cycloadducts for testing as organocatalysts, the [3+2] cycloaddition reaction starting from imine **7a** and β-nitrostyrene (**8a**) was carried out in the presence of silver acetate and triethylamine. In this case, a mixture of racemic *endo*-, *exo*-, and *exo'*-*rac*-**4aa** cycloadducts was obtained (Scheme 4), from which the minor isomer *exo'*-*rac*-**4aa** was separated by column chromatography on silica gel. This racemic compound was then subjected to preparative resolution by HPLC with a chiral column, which allowed the isolation of *exo'*-L-**4aa** and *exo'*-D-**4aa** in optically pure form (see the Supporting Information). Assignment of the absolute configurations of the resolved enantiomers was carried out by transformation of the first-eluting enantiomer (*exo'*-L-**4aa**) into the corresponding *N*-(4-bromobenzoyl) derivative *exo'*-L-**10aa** (Scheme 4) and resolution of the crystalline structure of this compound by X-ray diffraction analysis.[29]

Kinetic Studies

In order to assess the organocatalytic activity of the synthesized unnatural proline esters L-**4**, we chose as a case study the aldol reaction between cyclohexanone (**1a**) and pentafluorobenzaldehyde (**2a**). In principle, four isomeric adducts **3aa** can be expected for this reaction (Scheme 5).

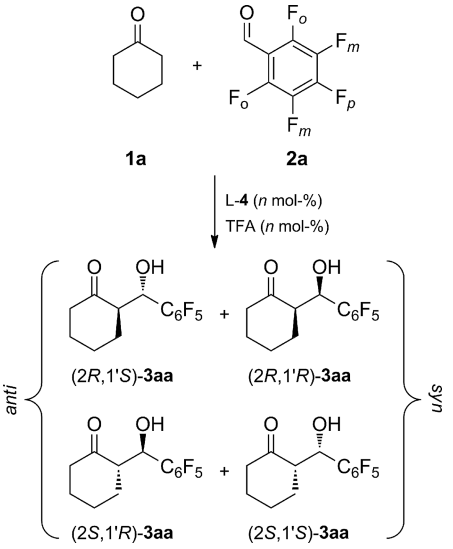

Scheme 5. Model aldol reaction to assess the organocatalytic activity of cycloadducts **4**. Descriptors *o*, *m* and *p* denote *ortho*, *meta* and *para* positions with respect to the carbaldehyde group.

Preliminary studies[26] showed that **2a** is quite electrophilic, and therefore the progress of the aldol reaction in the presence of different organocatalysts can be monitored in relatively short reaction times. In addition, the presence of fluorine atoms in *ortho*, *meta*, and *para* positions with respect to the carbaldehyde group (Figure 2) allows monitoring of the evolution of the reaction mixtures by ^{19}F NMR spectroscopy. The different signals were assigned by measuring the $^{3}J_{F,F}$ and $^{4}J_{F,F}$ coupling constants (see the Supporting Information). Figure 2 (A) shows the spectra registered for the reaction between **1a** and **2a** in the presence of *exo*-L-**4aa** with a catalytic load of 30 mol-% at 298 K. Together with the consumption of the starting aldehyde **2a**, formation of the major and minor adducts *anti*-**3aa** and *syn*-**3aa**, respectively, can be observed. Moreover, transient formation of iminium intermediates **INT2a** (Scheme 1) can be detected under these conditions (Figure 2).

In order to monitor the presence of enamine intermediates of type **INT1** (Scheme 1) by this method, at least one fluorine atom must be present in the catalyst. We therefore studied the same reaction in the presence of *exo*-L-**4ea** (Figure 3). In this case, aside from the ensemble of signals between –140 and –165 ppm associated with the C_6F_5 moiety (Figure 2), both enamine intermediates **INT1b** and **INT2b** were detected between –113 ppm and –115 ppm, together

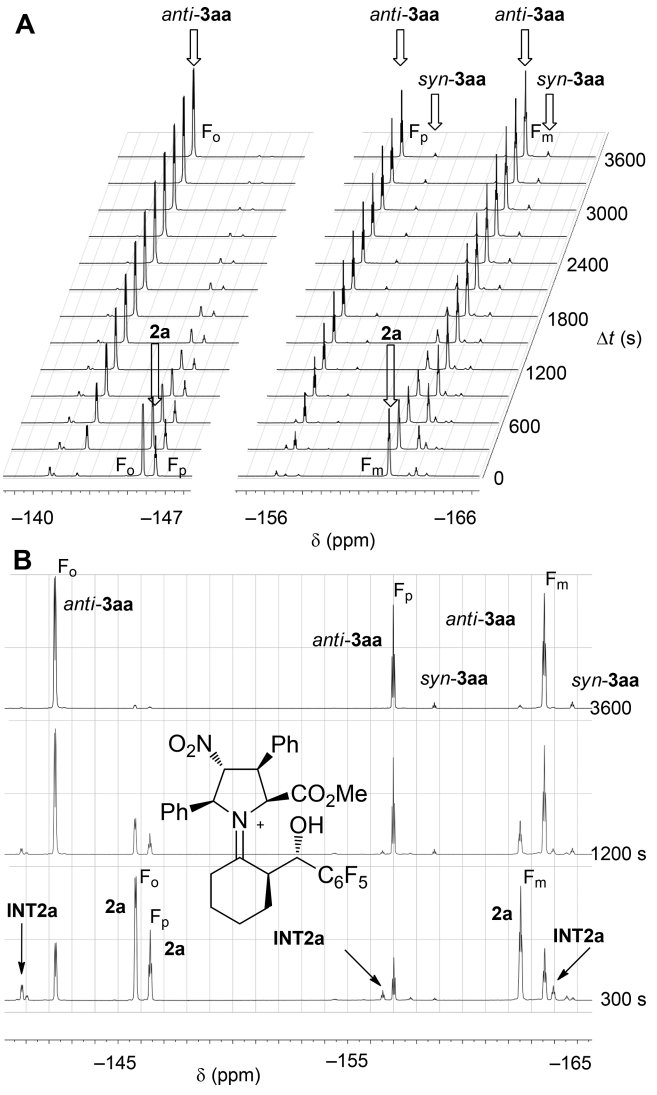

Figure 2. (A) ^{19}F NMR spectra obtained for the aldol reaction between **1a** and **2a** to form adducts **3aa**, catalyzed by *exo*-L-**4aa**. The hollow arrows show the decay of the signals corresponding to **2a**. These decays were used to estimate the kinetic constants. (B) Three selected spectra showing the evolution of reactants, products, and iminium intermediate **INT2a** (Figure 1).

with the broad signal corresponding to *exo*-L-**4ea** (Figure 3). These observations are compatible with the catalytic cycle depicted in Figure 1, because both enamine and iminium aldol intermediates were detected, the latter being more persistent. This suggests that, most likely, the hydrolytic step (stage III, Figure 1) is kinetically slower than the formation of the nucleophilic enamine.

With this information, we undertook the determination of the kinetic constants associated with the **1a** + **2a** → **3aa** reaction in the presence of different organocatalysts. Because the previously discussed ^{19}F NMR studies had suggested a kinetically complex profile, we decided to work under pseudo-first order conditions, with a **1a**/**2a** ratio of 60:1. The apparent reaction rates were measured according to Equation (1).

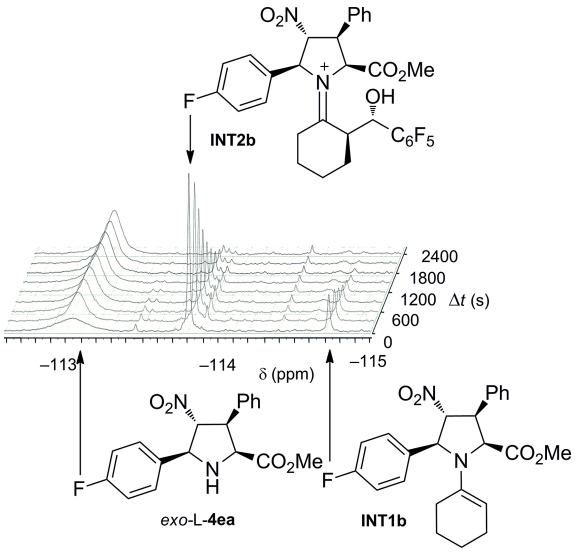

Figure 3. ^{19}F NMR spectra associated with the aldol reaction between **1a** and **2a** catalyzed by *exo*-L-**4ea**, showing the evolution of the catalyst, enamine intermediate **INT1b**, and iminium intermediate **INT2b**.

$$rate = -\frac{d[2a]}{dt} \approx k_{obs}[2a] \quad (1)$$

As internal reference we used the signal corresponding to trifluoroacetic acid (TFA). For each signal associated with *ortho*, *meta*, and *para* fluorine atoms of **2a**, we monitored the decay of the corresponding integrals (Figure 2, A) by means of Equation (2)

$$\ln\left(\frac{I_t^i}{I_t^{TFA}}\right) - \ln\left(\frac{I_0^i}{I_o^{TFA}}\right) = -k_{obs}t \quad (2)$$

where I_t^i and I_0^i are the instant and initial integrals, respectively, of the *i*-fluorine atom of **2a**. The experimental measurements were averaged for the three sets of signals associated with the *ortho*, *meta*, and *para* fluorine atoms of **2a**. Figure 4 (A) shows the conversion of **1a** and **2a** into **3aa** in the presence of organocatalysts *exo*-L-**4aa**, *endo*-L-**4aa**, and *exo′*-L-**4aa**. Figure 4 (B) shows the linear plot obtained after application of Equation (2). Similar excellent correlations were obtained in the remaining cases, thus showing pseudo-first order behavior of the studied reactions (see the Supporting Information). The kinetic constants calculated from treatment of NMR spectroscopic data by application of Equation (2) are collected in Table 1.

Our results indicate that, for the different L-**4aa** stereoisomers tested, the catalytic activity order is *exo* > *endo* >> *exo′*. Therefore, although the configurations of the *C*2 and *C*5 positions contiguous to the *N*1 active site of the pyrrolidine ring are identical in the three cases, the stereochemistry at the distal *C*3 and *C*4 atoms has a considerable effect on the rate of the aldol reaction. In particular, the relative *cis* configuration of the phenyl and nitro groups in *exo′*-L-**4aa** results in a significantly lower kinetic constant (Table 1, Entry 4).

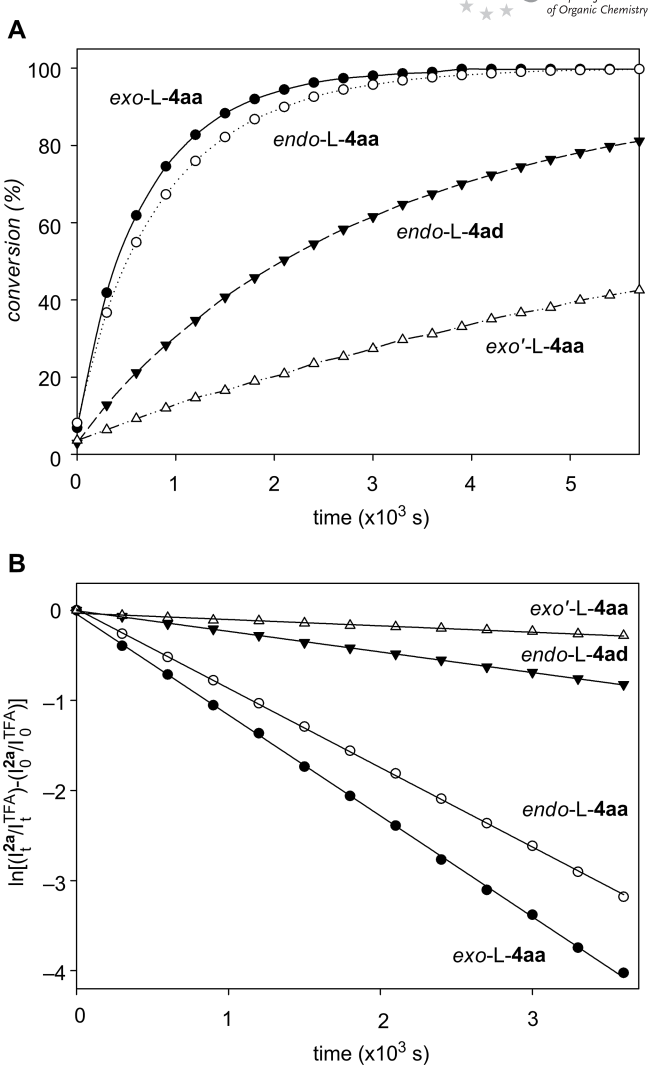

Figure 4. (A) Levels of conversion over time associated with the **1a** + **2a**→**3aa** transformation in the presence of organocatalysts *exo*-L-**4aa**, *endo*-L-**4aa**, *exo′*-L-**4aa**, and *endo*-L-**4ad**. All reactions were monitored under pseudo-first order conditions at 25 °C by ^{19}F NMR (see text). (B) Pseudo-first order linear plots obtained for the organocatalyzed reactions shown in (A). These plots were used to determine k_{obs} (see text).

In order to confirm this result with an *endo*-cycloadduct possessing *cis* substituents at *C*3 and *C*4, we measured the k_{obs} value for *endo*-L-**4ad** and also observed a relatively low kinetic constant (Table 1, Entry 5). Therefore, we conclude that a *cis* relationship between the substituents at *C*3 and *C*4 results in a lower organocatalytic activity. It is also noteworthy that *exo*-L-**4aa** retains a significantly high k_{obs} value with a catalytic load of 5 mol-% (Table 1, Entry 2).

In order to assess the role of TFA in general or specific co-catalytic schemes[30] we measured the values of k_{obs} for the **1a** + **2a**→**3aa** reaction catalyzed by *exo*-L-**4aa** in the presence of different TFA concentrations. The results are collected in Table 2, in which we have included the k_{obs} value in the absence of acid. This value (Table 2, Entry 1)

Table 1. Measured catalytic constants (k_{obs}) for cycloadducts *exo*-L-**4aa**, *endo*-L-**4aa**, *exo'*-L-**4aa**, and *endo*-L-**4ad** in the **1a** + **2a** → **3aa** reaction.[a,b]

Entry	Cat.	Cat. structure	Cat. load (mol-%)	k_{obs} ($\times 10^{-4}$ s^{-1})
1	*exo*-L-**4aa**	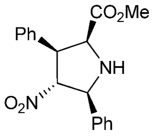	30	11.29 (±0.30)
2			5	3.67 (±0.06)
3	*endo*-L-**4aa**	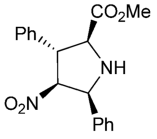	30	8.83 (±0.16)
4	*exo'*-L-**4aa**	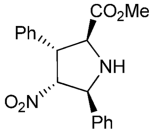	30	0.67 (±0.01)
5	*endo*-L-**4ad**	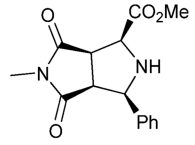	30	2.24 (±0.02)

[a] Pseudo-first order constants calculated by application of Equation (2) with a **1a**/**2a** ratio of 60:1. [b] All reactions were monitored by ^{19}F NMR at 25 °C.

was found to be two to three orders of magnitude lower than those observed when TFA was added (Table 2, Entries 4–11). Other carboxylic acids such as acetic acid and 4-nitrobenzoic acid promoted smaller enhancements of the k_{obs} values. Therefore, TFA proved to be a convenient acidic additive for this reaction. In addition, according to our experiments with variable concentrations of TFA, a roughly linear behavior of k_{obs} with respect to [TFA] is observed for acid concentrations within the catalytic range (i.e., close to or lower than 30 mol-% with respect to the limiting reactant

Table 2. Pseudo-first order experimentally measured[a,b] (k_{obs}) and calculated[c] (k_{calc}) kinetic constants measured for the **1a** + **2a** → **3aa** reaction catalyzed by *exo*-L-**4aa** with different acids and concentrations.

Entry	Acid	Mol-%	k_{obs} ($\times 10^{-4}$ s^{-1})
1	none	0	0.0429 (±0.0004)
2	AcOH	30	0.551 (±0.016)
3	PNB[c]	30	0.388 (±0.003)
4	TFA	15	6.37 (±0.14)
5	TFA	20	8.60 (±0.34)
6	TFA	25	10.00 (±0.29)
7	TFA	30	11.29 (±0.30)
8	TFA	50	15.73 (±0.35)
9	TFA	60	18.44 (±0.14)
10	TFA	75	21.88 (±0.19)
11	TFA	100	25.53 (±0.76)
12	TFA	150	26.75 (±0.06)

[a] Pseudo-first order constants calculated by application of Equation (2) with a **1a**/**2a** ratio of 60:1. [b] All reactions were monitored by ^{19}F NMR at 25 °C. [c] PNB: *p*-nitrobenzoic acid.

2a). For higher values, the measured k_{obs} values evolve towards a saturation profile.

We reasoned that the behavior reported in Table 2 could be described by Equation (3).

$$k_{obs} = k_0 + \frac{A[TFA]}{B + [TFA]} \quad (3)$$

In Equation (3), k_0 is the k_{obs} value for [TFA] = 0 (Table 2, Entry 1), and A and B are two constants that can be determined from the experimental data reported in Table 2. For low values of [TFA] (i.e., for [TFA] << *B*), Equation (3) can be approximated as $k_{obs} - k_0 \approx (A/B)$-[TFA], thus resulting in linear behavior. On the other hand, if [TFA] >> *B*, then Equation (3) approaches to a zero-slope profile in the form $k_{obs} - k_0 \approx A$, which would be associated with a maximum $k_{obs} - k_0$ value.

A double reciprocal treatment[31] of the data in Table 2 revealed a good linear regression (r^2 = 0.996) with $A = 47.40 \times 10^{-4}$ and B = 95.10, as can be seen in Figure 5. This result confirms that the hypothesis proposed in Equation (3) is reasonable for the concentrations tested in our experiments. A possible interpretation of these results is that, despite the complex, multistep mechanism required for the catalysis of these aldol reactions, at catalytic concentrations the proton transfer to the oxygen atom of the aldehyde is involved in the rate-limiting step. At higher concentrations of TFA, protonation of the aldehyde occurs prior to the step associated with the formation of the C–C bond, the protonated aldehyde being the effective electrophile.

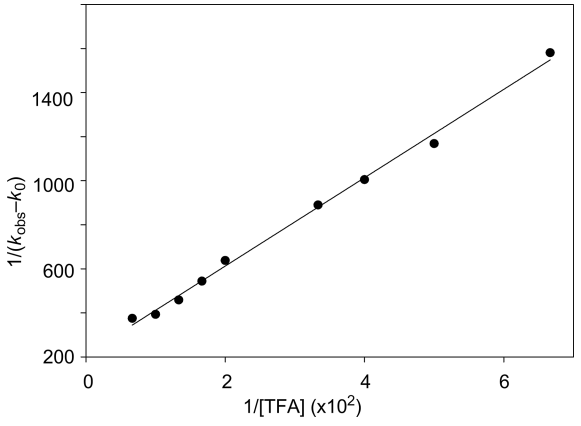

Figure 5. Double reciprocal treatment of the pseudo-first order constants (k_{obs}) reported in Table 2.

Kinetic isotope effects (KIEs) were measured for the **1a** + **2a** → **3aa** reaction catalyzed by *exo*-L-**4aa**. The results are collected in Table 3. When the reaction was performed in the presence of α,α,α′,α′-tetradeuterated cyclohexanone **1a**-d_4, a KIE of 2.68 was observed (Table 3, Entry 1). This value is between the KIE reported for the nornicotin-catalyzed aldol reaction between acetone and 4-nitrobenzaldehyde, for which Janda et al.[32] measured a KIE of 3.0 in the presence of D_2O, and the KIE ≈ 2 found by Blackmond et al.[33] for the L-Pro-catalyzed reaction between [D_6]acetone and 3-chlorobenzaldehyde.

Table 3. Kinetic isotope experiments conducted[a] for the **1a** + **2a** → **3aa** reaction catalyzed by cycloadduct *exo*-L-**4aa**.

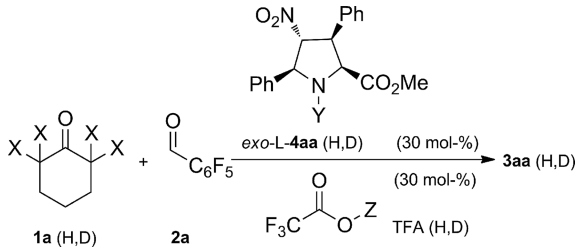

Entry	X	Y	Z	k_{obs} ($\times 10^{-4}$ s^{-1})	k_H/k_D[b]
1	D	H	H	4.21 (±0.29)	2.68 (±0.20)
2	H	D	H	7.61 (±0.22)	1.48 (±0.06)
3	H	H	D	11.59 (±0.22)	0.97 (±0.03)
4	H	D	D	7.36 (±0.51)	1.53 (±0.11)
5	D	D	D	3.16 (±0.24)	3.57 (±0.29)

[a] All reactions were conducted in neat **1a** at 25 °C with a **1a**/**2a** ratio of 60:1. Reference value: k_H = 11.29 × 10^{-4} (± 0.30) (see Table 1). [b] Errors were calculated from standard deviations of the rate constants according to ref.[34]

In the presence of *N*-deuterated *exo*-L-**4aa**, a significant normal KIE was detected (Table 3, Entry 2). When the acidic position of TFA was deuterated (Table 3, Entry 3) we were unable to measure any noticeable KIE within the experimental error. In line with these two results, deuteration of the acidic positions of both *exo*-L-**4aa** and TFA resulted in a normal KIE similar to that found when only the *NH*-site of *exo*-L-**4aa** was deuterated (Table 3, Entries 2 and 4). Finally, deuteration at the four α-positions of **1a** and of the acidic sites in *exo*-L-**4aa** and TFA resulted in a KIE of 3.57 (Table 3, Entry 5), a value larger than that measured in the presence of **1a**-d_4.

In summary, from the experiments reported in Table 3 we conclude that the observed KIE for the deuterated nucleophile is the outcome of a tradeoff between the large normal primary KIE associated with the formation of the enamine intermediate (Figure 1, stage I), the inverse secondary KIE expected for the C–C bond-forming step (Figure 1, stage II), and the normal primary KIE associated with the hydrolysis of the iminium aldol adduct (Figure 1, stage III), in the presence of enolization equilibria under general acid catalysis conditions within the 30 mol-% range (see Table 2). We can also conclude that stage II, associated with the formation of the C–C bond and hence with the stereocontrol of the aldol reaction, cannot be considered the rate-limiting step.

The diastereo- and enantioselectivities observed for the **1a** + **2a** → **3aa** reaction catalyzed by the three L-**4aa** cycloadducts were also measured, and the results are included in Table 4. In the case of *exo*-L-**4aa**, an excellent *anti* selectivity was observed. A catalytic load of 5 mol-% was not detrimental in terms of stereocontrol and chemical yield (Table 4, Entries 1 and 2). In addition, the enantiomeric excess (*ee*) was slightly better at –15 °C (Table 4, Entry 3). When acetic acid and 4-nitrobenzoic acids were used as additives in the presence of *exo*-L-**4aa** (Table 4, Entries 4 and 5), the measured *ee* values were slightly lower than those obtained with TFA, thus confirming the superior performance of this last additive, not only in terms of kinetic acceleration (vide supra), but also in terms of stereocontrol. Cycloadducts *endo*-L-**4aa** and *endo*-L-**4ad** gave good *syn*/*anti* diastereocontrol and chemical yields (Table 4, Entries 6, 7, and 9). Surprisingly, the sense of chiral induction of *endo*-L-**4aa**, *exo′*-L-**4aa**, and *endo*-L-**4ad** was found to be the opposite of that observed for *exo*-L-**4aa**. This unexpected result is discussed later on. Finally, it is worth noting that *exo′*-L-**4aa** and *endo*-L-**4ad**, with *cis* substituents at *C*3 and *C*4, give poor enantiocontrol, the former also showing a low *syn*/*anti* diastereoselectivity (Table 4, Entries 8 and 9). Therefore, these two compounds are not convenient in terms of organocatalytic activity (vide supra) and stereocontrol.

Table 4. Stereocontrol and chemical yields observed[a] in the **1a** + **2a** → **3aa** reaction catalyzed by cycloadducts *exo*-L-**4aa**, *endo*-L-**4aa**, *exo′*-L-**4aa**, and *endo*-L-**4ad** in the presence of TFA (30 mol-%).

Entry	Cat.	*T* [°C]	Cat. load [mol-%]	*anti*/*syn*[b]	Yield[c] [%]	*ee*[d] [%]
1[e]	*exo*-L-**4aa**	25	30	95:05	73	89[d]
2		25	5	95:05	81	89
3[e]		–15	30	99:01	70	92
4[f]		25	30	97:03	73	81
5[g]		25	30	96:04	69	78
6	*endo*-L-**4aa**	25	30	96:04	83	–81
7		–15	30	99:01	80	–84
8	*exo′*-L-**4aa**	25	30	42:58	75	–24
9	*endo*-L-**4ad**	25	30	92:08	85	–47

[a] Determined on crude reaction mixtures after >99% conversion. [b] Determined by ^{1}H or ^{19}F NMR on crude reaction mixtures. [c] Isolated yields of *anti* and *syn* aldols after workup. [d] Determined by HPLC with chiral stationary phases and computed as *ee* = 100 × [(2*R*,1′*S*) – (2*S*,1′*R*)]/[(2*R*,1′*S*)+(2*S*,1′*R*)]. [e] Results reported in [26]. [f] Acetic acid was used as additive. [g] 4-Nitrobenzoic acid was used as additive.

We also investigated the effect of including *para*-substituents on the 3,5-diphenyl groups of *exo*-L-**4aa**. To this end, the behavior of cycloadducts *exo*-L-**4ea**–**dc** was analyzed. The results are reported in Table 5. All these compounds provided satisfactory chemical yields and *anti*/*syn* diastereoselectivities. Interestingly enough, these effects do not seem to be additive, because neither two fluorine atoms (Table 5, Entry 5) nor one methoxy and one fluorine substituent (Table 5, Entry 6) produced k_{obs} values higher than those obtained with the monosubstituted cycloadducts. Despite the modest acceleration observed with respect to *exo*-L-**4aa**, the measured enantiomeric excesses were found to be slightly lower than those found for the parent catalyst.

We next explored other substitution patterns in cycloadducts *exo*-L-**4**. In Table 6 we report the results obtained with respect to L-Pro. We observed that the free amino acid *exo*-L-**4′aa**, obtained by hydrolysis of methyl ester *exo*-L-**4aa** (Scheme 3), retains the *anti*/*syn* diastereoselectivity and the sense of enantioselection, although with a slightly lower enantiomeric excess and chemical yield (Table 6, Entry 3). In the case of *endo*-L-**4′aa** (Table 6, Entry 3), the *ee* has the same sign as observed with the naturally occurring L-Pro

Table 5. Pseudo-first[a] order kinetic constants (k_{obs}), chemical yields,[b] and enantiomeric excesses (*ee*)[c] observed in reaction **1a** + **2a** → **3aa** catalyzed by compounds *exo*-L-**4ea**–**dc**.

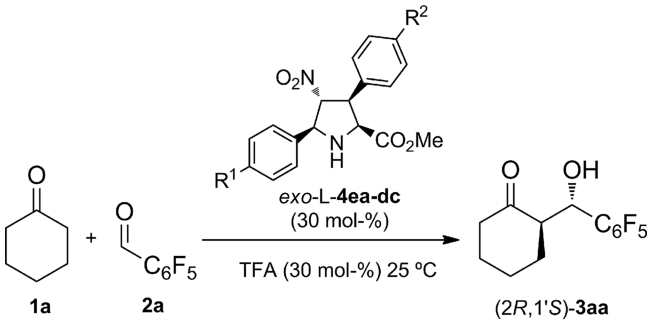

Entry	Cat.	R^1	R^2	Yield [%]	*ee* [%]	k_{obs} ($\times 10^{-4}$ s^{-1})
1	*exo*-L-**4ea**	F	H	80	78	6.23 (±0.19)
2	*exo*-L-**4ac**	H	F	72	83	10.18 (±0.36)
3	*exo*-L-**4da**	OMe	H	68	77	11.28 (±0.35)
4	*exo*-L-**4ab**	H	OMe	78	87	14.74 (±0.78)
5	*exo*-L-**4ec**	F	F	88	81	5.59 (±0.08)
6	*exo*-L-**4dc**	OMe	F	79	76	8.64 (±0.35)

[a] All reactions were monitored at 25 °C with a **1a**/**2a** ratio of 60:1 until conversion >99%. In each case the *anti*/*syn* ratio was about 95:5. [b] Isolated yields of **3aa**. [c] Enantiomeric excesses corresponding to the major *anti* diastereomer were determined by HPLC and computed as *ee* = 100 × [(2*R*,1′*S*) – (2*S*,1′*R*)]/[(2*R*,1′*S*) + (2*S*,1′*R*)].

(Table 6, Entry 1). This change in the sense of chiral induction is discussed in more detail below. The presence of an alkoxy group bulkier than a methoxy group (compound *exo*-L-**4ba**, Table 6, Entry 4) also resulted in a lower *ee* and chemical yield. This detrimental effect was more pronounced in the case of a 2-naphthyl group at *C*5 (compound *exo*-L-**4ca**, Table 6, Entry 5). Finally, we found that either a quaternary group at *C*2 or a *tert*-butyl group at *C*5 (compounds *exo*-L-**4ha**, *exo*-L-**4ia**, and *exo*-L-**4fa**) resulted in an almost complete loss of organocatalytic activity (Table 6, Entries 6–9). Therefore, the substitution patterns included in Entries 4–9 of Table 6 should be avoided in the development of other catalysts based on this scaffold.

We also tested the stereoselectivity and catalytic efficiency of selected compounds **4** in the absence of any acid additive. The results are reported in Table 7 and indicate that under these conditions the reaction times required for esters *exo*- and *endo*-L-**4aa** are much longer (Entries 1 and 2). In addition, the *ee* values are considerably lower, although the sense of induction was that obtained in the presence of TFA or other acids. In the case of acids *exo*-L-**4′aa** and *endo*-L-**4′aa** (Entries 3 and 4) the reaction times were considerably shorter than those observed with the corresponding esters. In addition, the *ee* values were also lower than those achieved with the corresponding esters in the presence of TFA (Table 6, Entries 2 and 3). However, it is noteworthy that the sense of chiral induction of these compounds is the same as observed for the corresponding esters in the presence of TFA. These results confirmed that the most convenient reaction conditions correspond to the unnatural proline esters **4** with TFA (30 mol-%), in terms of

Table 6. Stereocontrol and chemical yields observed[a] in the **1a** + **2a** → **3aa** reaction catalyzed by L-Pro and by substituted *exo*-L-**4** cycloadducts (30 mol-%) in the presence of TFA (30 mol-%).

Entry	Cat.	T[a] (°C)	Conv. (%)	*anti*:*syn*	Yield[b] (%)	*ee*[c] (%)
1	L-Pro	25	>99	>95:05	70	–88
2	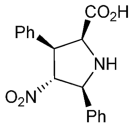 *exo*-L-**4′aa**	25	>99	90:10	65	86
3	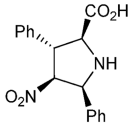 *endo*-L-**4′aa**	25	>99	92:08	70	–83
4	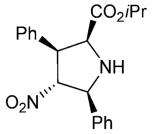 *exo*-L-**4ba**	–15	>99	92:08	40	63
5	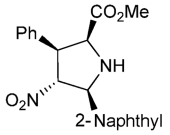 *exo*-L-**4ca**	–15	>99	>99:01	35	49
6	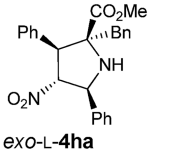 *exo*-L-**4ha**	–15	<5[d]	n.d.	n.d.	n.d.
7	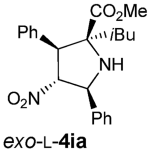 *exo*-L-**4ia**	–15	<1[d]	n.d.	n.d.	n.d.
8	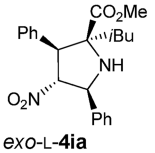 *exo*-L-**4ia**	25	<10[d]	n.d.	n.d.	n.d.
9	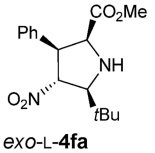 *exo*-L-**4fa**	25	35[d]	53:47	n.d.	12

[a] All reactions were monitored for 24 h, with a **1a**/**2a** ratio of 60:1. [b] Isolated yields of **3aa**. [c] Enantiomeric excesses corresponding to the *anti* diastereomer were determined by HPLC on crude reaction mixtures and computed as *ee* = 100 × [(2*R*,1′*S*) – (2*S*,1′*R*)]/[(2*R*,1′*S*) + (2*S*,1′*R*)]. [d] Observed levels of conversion after 48 h.

stereocontrol, reaction rate, and preparative simplicity of the synthetic organocatalysts.

Table 7. Stereocontrol and chemical yields observed[a] in the **1a** + **2a**→**3aa** reaction catalyzed by substituted *exo*- and *endo*-L-**4aa**, *exo*-L-**4′aa**, and *endo*-L-**4′aa** cycloadducts without acidic additives.

Entry	Cat.	*t* (h)	*anti*:*syn*	Yield[b] (%)	*ee*[c] (%)
1	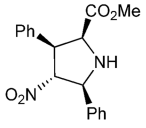 *exo*-L-**4aa**	144	97:3	78	71
2	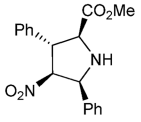 *endo*-L-**4aa**	144	98:2	72	–56
3	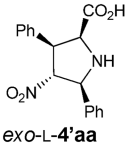 *exo*-L-**4′aa**	24	92:8	75	48
4	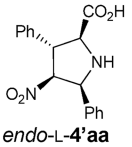 *endo*-L-**4′aa**	24	96:4	71	–55

[a] All reactions were monitored at 25 °C with a **1a**/**2a** ratio of 60:1 until 99% conversion. [b] Isolated yields of **3aa**. [c] Enantiomeric excesses corresponding to the *anti* diastereomer were determined by HPLC on crude reaction mixtures and computed as *ee* = 100 × [(2*R*,1′*S*) – (2*S*,1′*R*)]/[(2*R*,1′*S*) + (2*S*,1′*R*)].

Stereoselectivity of Organocatalysts *exo*-L-4aa and *endo*-L-4aa

In Table 4 we reported that *exo*-L-**4aa** yields the aldol adduct (2*R*,1′*S*)-**3aa** as the major stereoisomer of the **1a** + **2a**→**3aa** reaction, with 92% *ee* at –15 °C. In contrast, *endo*-L-**4aa** yields (2*S*,1′*R*)-**3aa** as the major adduct, with 84% *ee* under the same reaction conditions. The latter adduct is the enantiomer obtained in the presence of natural L-Pro (Table 6, Entry 1). In order to explore the persistence of this enantiodivergent behavior for *exo*-L-**4aa** and *endo*-L-**4aa**, we studied different aldol reactions involving ketones **1a**–**c** and aldehydes **2a**–**f** (Scheme 6). The results obtained are collected in Table 7.

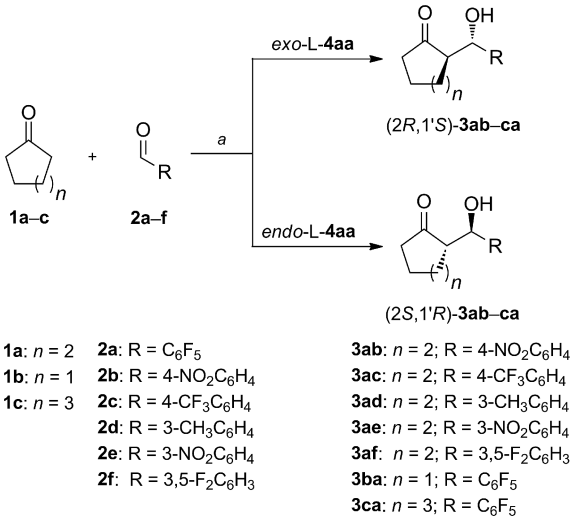

Scheme 6. Aldol reactions between ketones **1a**–**c** and aldehydes **2a**–**f** catalyzed by *endo*-L-**4aa** and *exo*-L-**4aa**. Reagents and conditions: (a) organocatalyst (30 mol-%), TFA (30 mol-%), –15 or +25 °C, 24 h (see Table 7).

Consistent behavior was observed for reactions between cyclohexanone (**1a**) and aldehydes **2a**–**f** (Tables 4 and 8). Thus, in the presence of organocatalyst *exo*-L-**4aa**, aldol adducts (2*R*,1′*S*)-**3aa**–**af** were obtained with *ee* values of about 90%. In comparison, use of *endo*-L-**4aa** provided the enantiomeric adducts (2*S*,1′*R*)-**3aa**–**af** as major isomers, with slightly lower enantiomeric excesses. Cyclopentanone

Table 8. Stereocontrol and chemical yields observed[a,b] in the **1a**–**c** + **2a**–**f**→**3ab**–**ca** reactions (Scheme 6) catalyzed by cycloadducts *exo*-L-**4aa** and *endo*-L-**4aa**.

Entry	*n*	R	Cat.	Aldol	*anti*/*syn*[c]	Yield [%]	*ee*[d] [%]
1[a]	2	4-$NO_2C_6H_4$	*exo*-L-**4aa**	(2*R*,1′*S*)-**3ab**	85:15	81[e]	92
2[a]	2	4-$NO_2C_6H_4$	*endo*-L-**4aa**	(2*S*,1′*R*)-**3ab**	88:12	84[e]	–90
3[a]	2	4-$CF_3C_6H_4$	*exo*-L-**4aa**	(2*R*,1′*S*)-**3ac**	86:14	79[e]	94
4[a]	2	4-$CF_3C_6H_4$	*endo*-L-**4aa**	(2*S*,1′*R*)-**3ac**	85:15	83[e]	–70
5[a]	2	3-MeC_6H_4	*exo*-L-**4aa**	(2*R*,1′*S*)-**3ad**	85:15	70[e]	92
6[a]	2	3-MeC_6H_4	*endo*-L-**4aa**	(2*S*,1′*R*)-**3ad**	83:17	75[e]	–66
7[a]	2	3-$NO_2C_6H_4$	*exo*-L-**4aa**	(2*R*,1′*S*)-**3ae**	80:20	60[e]	94
8[a]	2	3-$NO_2C_6H_4$	*endo*-L-**4aa**	(2*S*,1′*R*)-**3ae**	80:20	65[e]	–64
9[a]	2	3,5-$F_2C_6H_3$	*exo*-L-**4aa**	(2*R*,1′*S*)-**3af**	85:15	55[e]	86
10[a]	2	3,5-$F_2C_6H_3$	*endo*-L-**4aa**	(2*S*,1′*R*)-**3af**	83:17	67[e]	–74
11[b]	1	C_6F_5	*exo*-L-**4aa**	(2*R*,1′*S*)-**3ba**	82:18	65[e]	15
12[b]	1	C_6F_5	*endo*-L-**4aa**	(2*S*,1′*R*)-**3ba**	89:11	45[e]	–10
13[b]	3	C_6F_5	*exo*-L-**4aa**	(2*R*,1′*S*)-**3ca**	99:01	40[f]	59
14[b]	3	C_6F_5	*endo*-L-**4aa**	(2*S*,1′*R*)-**3ca**	99:01	84[f]	–35

[a] Reactions carried out at –15 °C. [b] Reactions carried out at 25 °C. [c] Ratios determined by ^{1}H NMR examination of the crude reaction mixtures. [d] Enantiomeric excesses corresponding to the major *anti* aldol adducts determined by HPLC with a chiral stationary phase and computed as *ee* = 100 × [(2*R*,1′*S*) – (2*S*,1′*R*)]/[(2*R*,1′*S*) + (2*S*,1′*R*)]. [e] Yields of isolated aldol adducts after conversion > 99%. [f] Yields of isolated aldol adducts after 48 h with conversion of 96%.

(**1b**) was more reactive than **1a**, but the enantiocontrol was found to be much lower (Table 8, Entries 11 and 12). The stereoselectivity observed with cycloheptanone (**1c**) was also lower than that found with **1a**, although the enantiocontrol was somewhat higher than that obtained for **1b** (Table 8, Entries 13 and 14). Therefore, cyclohexanone appears to represent a good compromise between reactivity and enantiocontrol in these reactions.

From these results it is clear that the stereochemical behavior of *exo*-L-**4aa**–**ec** (see also Table 5 and Table 6) is exceptional and completely different from that observed for L-Pro itself and other organocatalysts such as *endo*-L-**4aa**, *exo*′-L-**4aa**, and *endo*-L-**4ad**. In order to understand the reasons for this unexpected outcome, we decided to undertake a computational study of the model aldol reaction **1a** + **2a** → **3aa** in the presence of *exo*-L-**4aa** and *endo*-L-**4aa**. According to the accepted model for this reaction, the stereochemically relevant step is C–C bond formation from the enamine intermediates of type **INT1** and aldehydes **2**. In the case of the **1a** + **2a** → **3aa** reaction, the enamine intermediate can exist in two families of conformers **INT1a** and **INT1′a** depending on the *s-cis* or *s-trans* disposition, respectively, between the double bond of the enamine moiety and the methoxycarbonyl group (Scheme 7).

If we define the dihedral angle ω as ω = C*a*-N*b*-C*c*-C*d* (Figure 6), *s-cis* conformations will be obtained for ω values between 0 and ±75 deg., whereas *s-trans* conformations can be grouped for ω&epsis;(±95, ±180). MM3 molecular dynamics (MD) simulations (Figure 6) show different behavior of intermediates *exo*-**INT1a** and *endo*-**INT1a**, although in both cases both conformations are significantly populated. Both MD and Monte Carlo simulations show a remarkable conformational rigidity in the pyrrolidine ring, with three substituents occupying equatorial positions and one being isoclinal. In contrast, the cyclohexenyl moiety is much more flexible. At the M06–2X(PCM)/6–31+G**//B3LYP(PCM)/6–31G*+ΔZPVE level, *exo*-**INT1a** was calculated to be 0.4 kcal mol^{-1} less stable than the *exo*-**INT1′a** conformer, whereas the reverse relative stability was found for the *endo* analogues (see Figure S5 in the Supporting Information). Therefore, from these analyses, no general kinetic stereoselectivity trends can be envisaged for the aldol reaction in the presence of organocatalysts *exo*-L-**4aa** and *endo*-L-**4aa**.

If we consider the interaction pathways of the intermediate *exo*-**INT1a**, derived from *exo*-L-**4aa** with aldehyde **2a**, in principle these interactions can occur through both the nitro and methoxycarbonyl (X = Me) or carboxy (X = H) groups, as depicted in Scheme 7. In addition, depending upon the reaction conditions, the elementary step leading to the formation of the C–C bond can involve different Y-species. Thus, under non-acidic conditions Y can be H_2O (formed as a consequence of the generation of *exo*-**INT1a** in situ) or nothing. Similarly, reaction conditions including acidic additives can give rise to structures in which Y = H^+ or H_3O^+ (Scheme 7). The possible combinations generate a very complex situation in which many alternative transition structures can be present. However, intensive searching of

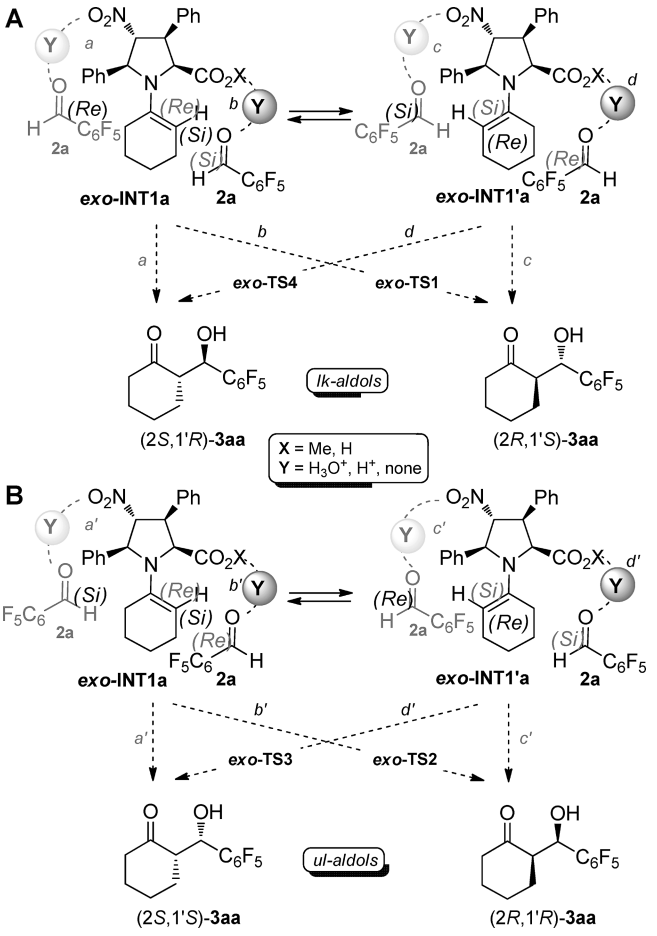

Scheme 7. (A) "Like" reaction path, and (B) "unlike" reaction path associated with the C–C bond-forming step of the aldol reaction between cyclohexanone and pentafluorobenzaldehyde (**2a**) in the presence of organocatalyst *exo*-L-**4aa**.

these saddle points along different topologies at the B3LYP(PCM = cyclohexanone)/6–31G* level of theory met with no success in the case of the interaction of **2a** with *exo*-**INT1a** through the nitro group (paths *a*, *a*′, *b*, and *b*′, Scheme 7) when X = OMe and Y = nothing, H^+. For Y = H_3O^+, saddle points associated with interaction patterns *a* and *c* through the nitro group were located, but were found to lie ca. 4 kcal mol^{-1} above their analogues *exo*-**TS1** and *exo*-**TS4** (see Figure S6 in the Supporting Information), in which the interaction between *exo*-**INT1a** and **2a** takes place through the methoxycarbonyl group (Scheme 7, interaction modes *b* and *d*). Therefore, we will restrict the following discussion to transition structures involving X = H, Me and Y = H^+ through the interaction patterns *b*, *b*′, *d*, and *d*′ shown in Scheme 7.

The chief geometric features and relative energies of saddle points *exo*-**TS1**–**4** [M06–2X(PCM = cyclohexanone)/6-31+G**//B3LYP(PCM = cyclohexanone)/6-31G* level of theory] are shown in Figure 7. These transition structures show Houk–List geometries[23] in which three substituents of the pyrrolidine ring occupy equatorial positions in half-chair conformations and the methoxycarbonyl group, in general constrained by the hydrogen bond with

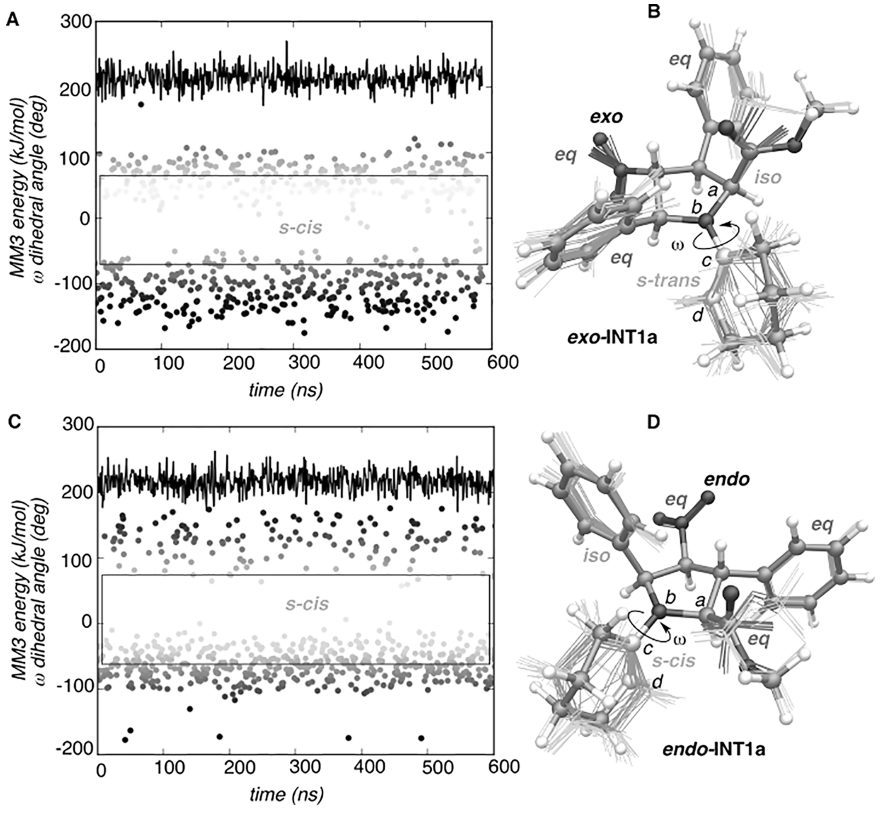

Figure 6. Molecular dynamics plots for (A) *exo*-**INT1a**, and (C) *endo*-**INT1a**, computed with use of the MM3 forcefield. The C*a*-N*b*-C*c*-C*d* dihedral angle is denoted ω. Areas denoted *s-cis* include structures for which $\omega \leq \pm 75$ deg. Monte Carlo conformational analyses calculated with MM3 for (B) *exo*-**INT1a**, and (D) *endo*-**INT1a**. Ball and stick representations correspond to the lowest-energy conformers, and the wire structures include the 20 most stable conformers within 2.6 and 2.9 kcal mol^{-1}, respectively.

the protonated aldehyde, occupies an isoclinal position (Figure 7). The Bürgi–Dunitz angles defined by *Cc*, C*b*, and the OH group vary from 100.5 to 106.9°. The dihedral angle ϕ defined as ϕ = C*a*-C*b*-*Cc*-C*d* (Figure 8) shows values close to +100° in *exo*-**TS2** and –100° in *exo*-**TS3.** This dihedral angle is closer to 180° in *exo*-**TS1** and *exo*-**TS4**. The former saddle point, which is the transition structure of lowest energy, shows an *s-cis* conformation of the enamine moiety and an antiperiplanar conformation of this group with respect to the C_6F_5 substituent, with ϕ = –174.1°, thus minimizing the steric repulsion generated by the 5-phenyl group of *exo*-L-**4aa**. These features make *exo*-**TS1** the least energetic transition structure associated with the C–C bond-forming step of the **1a** + **2a** → **3aa** reaction in the presence of organocatalyst *exo*-L-**4aa**. This transition structure leads to *anti*-aldol (2*R*,1′*S*)-**3aa**, in good agreement with the experimental results. The calculated *anti*/*syn* ratio is >99:01, and the computed *ee* for the *anti* isomers in the presence of *exo*-L-**4aa** is >99%. Both results are in qualitative agreement with the experimentally determined values of 95:05 and 89%, respectively (Table 4, Entries 1 and 2).

It is worth noting that when X = H and Y = none, the corresponding Houk–List saddle point *exo*-**TS1** is 0.8 kcal mol^{-1} lower in energy than its *exo*-**TS4** analogue (see Figure S7 in the Supporting Information), a result pleasingly in agreement with the experimentally observed lower *ee* for *exo*-L-**4′aa** in the absence of TFA (Table 7, Entry 4).

The transition structures *endo*-**TS1**–**4** associated with the **1a** + **2a** → **3aa** reaction catalyzed by *endo*-L-**4aa** (Figure 8) show non-optimal geometric features in all cases. Thus, *endo*-**TS1**–**3** each show one axial and two isoclinal groups in the pyrrolidine ring, and only *endo*-**TS4** is able to accommodate four equatorial substituents, but at the cost of a certain steric congestion between the C_6F_5 group and the equatorial phenyl group at *C*5 of the organocatalyst (Figure 8). This tradeoff between unfavorable features might be responsible for the slightly lower catalytic activity observed for *endo*-L-**4aa** (Figure 4 and Table 1, Entry 3). The reverse enantioselectivity observed for this catalyst with respect to *exo*-L-**4aa** is also compatible with the relative energies shown in Figure 8. Saddle point *endo*-**TS4** has suitable Bürgi–Dunitz and ϕ angles, the four substituents of the pyrrolidine ring being in equatorial positions. In addition, this transition structure can develop a strong hydrogen bond between the OH group being formed and the methoxycarbonyl group. However, the *s-trans* conformation of the cyclohexenyl moiety imposes a close proximity between the C_6F_5 group of the electrophile and the 5-phenyl group of *endo*-L-**4aa**. This unfavorable steric congestion does not overcome the other favorable features of *endo*-**TS4**, thus making this stationary point, which leads to *anti* aldol

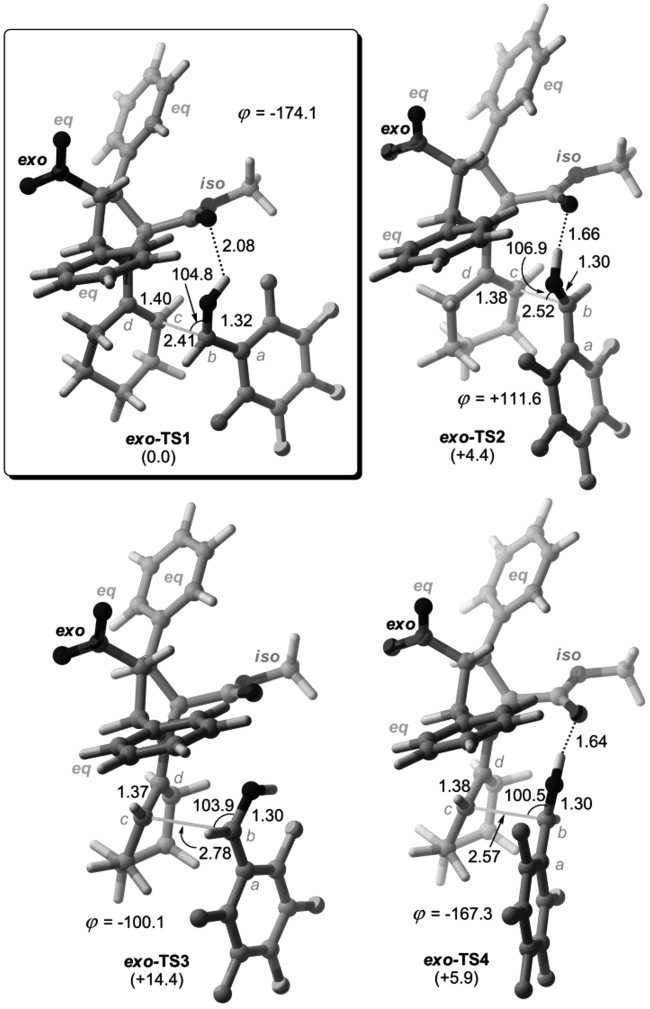

Figure 7. Chief features of transition structures *exo*-**TS1**–**4** fully optimized at the B3LYP(PCM)/6–31G* level of theory. Bond lengths and angles are given in Å and deg., respectively. The dihedral angle defined by C*a*, C*b*, C*c*, and C*d* atoms is denoted ϕ. Numbers in parentheses correspond to relative energies (in kcal mol^{-1}) computed at the M06-2X(PCM)/6-31+G**//B3LYP(PCM)/6-31G*+ΔZPVE level. Equatorial and isoclinal positions are denoted *eq* and *iso*, respectively.

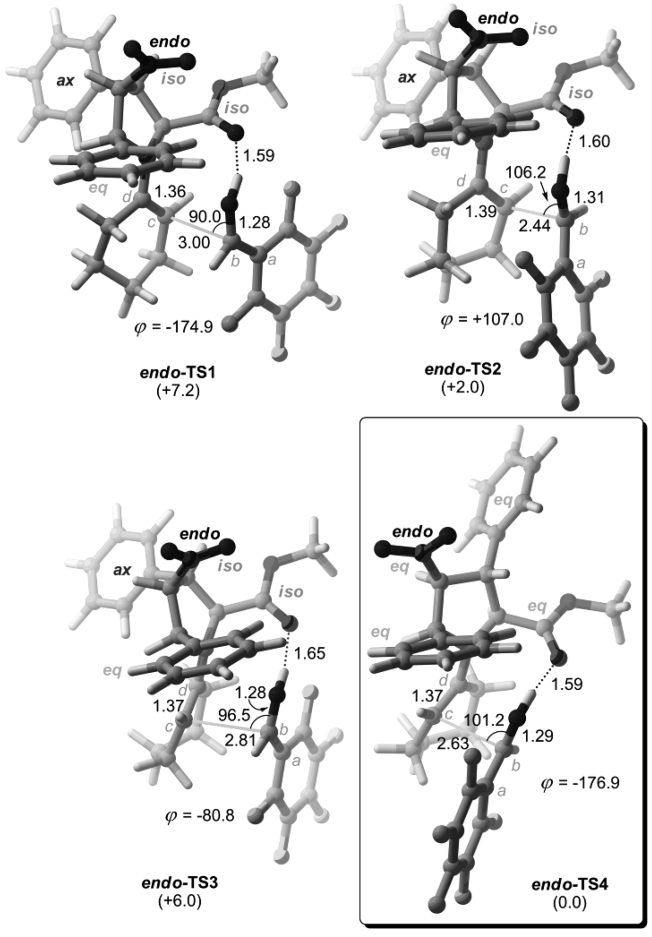

Figure 8. Chief features of transition structures *endo*-**TS1**–**4** fully optimized at the B3LYP(PCM)/6-31G* level of theory. See the caption of Figure 7 ■■ ((<=Author: change correct? was 8)) ■■ for further details.

(2*S*,1′*R*)-**3aa**, the lowest-energy saddle point of this series. The calculated *anti*/*syn* ratio at 298 K is 97:03 and the *ee* for the *anti* aldols is >99%. Once again, these results are in qualitative agreement with the experimental data at 298 K [96:04 and 81% (absolute value), respectively (Table 4, Entry 4)].

These combined experimental and computational data indicate that densely substituted proline-based organocatalysts can show unexpected organocatalytic properties. Thus, aside from the geometric and stereoelectronic effects imposed by the Houk–List geometries, subtle remote effects stemming from conformational preferences in the pyrrolidinone ring can result in unique asymmetric induction effects, not available for organocatalysts based on natural L-amino acids such as L-Pro.

Conclusions

From the experimental and computational data reported in this study the following conclusions can be drawn: (i) densely substituted unnatural proline esters, readily accessible through asymmetric [3+2] cycloadditions, can be used as efficient organocatalysts for aldol reactions, and methyl esters in the presence of TFA are superior to the corresponding acids in terms of accessibility, reaction rate, and stereocontrol, (ii) in these systems, substituents at positions *C*3 and *C*4 of the pyrrolidine ring must be *trans* to each other, (iii) quaternary centers at *C*2 destroy the catalytic activity, (iv) aryl groups at *C*5 are preferable to alkyl groups, (v) bulky alkoxycarbonyl groups at *C*2 must be avoided, (vi) the sense of induction of the organocatalysts depends on several factors (maximum number of equatorial substituents in the pyrrolidine ring, intramolecular hydrogen bonds, *gauche* disposition between the N–C=C and C=O bonds in the transition structure, and potential steric clash between the substituent at *C*5 and the substituent of the aldehyde), and (vii) according to the balance of these factors *exo*-L-proline esters preferentially yield *anti*

(2*R*,1′*S*) aldols, whereas the *endo* organocatalysts yield the corresponding (2*S*,1′*R*) aldols as major products.

Experimental Section

Determination of Pseudo-First Order Kinetic Constants: 2,3,4,5,6-Pentafluorobenzaldehyde (**2a**) (0.1 mmol, 20 mg, 1 equiv.) and the corresponding organocatalyst **4** (0.03 mmol, 0.3 equiv.) were dissolved in neat, freshly distilled (MS, 3 Å) cyclohexanone (**1a**, 0.63 mL, 6 mmol, 60 equiv.) at room temperature. This mixture was transferred to a NMR tube, and then trifluoroacetic acid (0.03 mmol, 2.3 μL, 0.3 equiv. in standard experiments) was added. The resulting mixtures were immediately introduced into the NMR probe. Samples were stabilized at 298 K. The kinetic studies were performed by monitoring the three ^{19}F NMR signals of free **2a**, together with the other signals also associated with the C_6F_5 group, obtained with inverse gate ^{1}H-decoupling. Trifluoroacetic acid (δ = –76 ppm) was used as internal reference. NMR measurements were carried out at 376.40 MHz with a Bruker Advance 400 NMR spectrometer, equipped with a BBOF probe incorporating *z*-gradients. FID files were obtained with a spectral window of 240 ppm and transformed with 65536 points. All spectra were recorded by accumulating 16 acquisitions, with recycling delays of 1 s. Measurements were performed directly on the reaction mixtures in the NMR tubes every 5 min. Relative concentrations of **2a** at different times were quantified by integration and statistical treatment of the three sets of ^{19}F signals. Kinetic constants reported in Tables 1, 2, 3, and 5 were obtained from the NMR experiments and application of Equation (2). All KIE experiments reported in Table 3 were carried out in triplicate and subjected to further statistical treatment.

Molecular Dynamics: The MD simulations of intermediates **INT1a** and **INT1′a** were carried out with use of the MM3 forcefield[35] as implemented in the MacroModel package.[36] Calculations were performed with SHAKE[37] to constrain the C–H bonds. The temperature was set up to 298 K. The system was equilibrated for 1 ns with time steps of 1 fs. The production run was started from this point and lasted another 600 nanoseconds with time steps of 1 fs. In all cases we observed that during the production period the energy and temperature of the whole system were equilibrated. During the production run, the coordinates of 500 structures were saved.

DFT Calculations: Density functional theory calculations were performed by use of the Gaussian 09 suite of programs.[38] Full geometry optimizations and harmonic analyses were carried out by use of the B3LYP hybrid functional[39] and the 6-31G* basis set. Solvent effects were computed by the PCM method[40] and with cyclohexanone as model solvent. Single-point energies were computed by use of the M06-2X functional[41] and the 6-31+G** basis set. Free energies were computed at 298.15 K.

Acknowledgments

Financial support was provided by the Spanish Ministerio de Economía y Competitividad (MINECO) and the Fondos Europeos para el Desarrollo Regional (FEDER) (projects CTQ2010-16959/BQU, CTQ2012-35535, CTQ2007-62771/BQU, CTQ2010-20387, CTQ2010-17436, and Consolider-Ingenio CSD2007-00006), the University of the Basque Country (UPV/EHU, UFI11/22 QOSYC), the Basque Government (GV/EJ, grant IT-324-07), the Generalitat Valenciana-FEDER (PROMETEO/2009/039), the Gobierno de Aragón-FSE (research group E40), and the University of Alicante. M. d. G. R. thanks the ####### (DIPC) ■■ ((<=Author: please add the sponsor name, written in full length)) ■■ for a postdoctoral contract. M. S. and L. C. gratefully thank MINECO for a contract funding their PhD projects. The authors thank the SGI/IZO-SGIker UPV/EHU and the DIPC for generous allocation of computational and analytical resources. Technical and human support provided by SGIker (UPV/EHU, MINECO, GV/EJ, ESF) is gratefully acknowledged.

[1] a) R. Mahrwald (Ed.), *Modern Methods in Stereoselective Aldol Reactions*, Wiley-VCH, Weinheim, Germany, **2011**; b) R. Mahrwald (Ed.), *Modern Aldol Reactions*, Wiley-VCH, New York, vol. 1 and 2.

[2] a) W.-D. Fessner, A. Schneider, H. Held, G. Sinerius, C. Walter, M. Hixon, J. V. Schloss, *Angew. Chem. Int. Ed. Engl.* **1996**, *35*, 2219–2221; *Angew. Chem.* **1996**, *108*, 2356–2358; b) L. J. Whalen, C.-H. Wong, *Aldrichim. Acta* **2006**, *39*, 63–71; c) T. D. Machajewski, C.-H. Wong, *Angew. Chem. Int. Ed.* **2000**, *39*, 1352–1375; *Angew. Chem.* **2000**, *112*, 1406–1429; d) D. J. Kuo, I. A. Rose, *Biochemistry* **1985**, *24*, 3947–3955; e) A. Heine, L. J. G. Luz, C.-H. Wong, I. A. Wilson, *J. Mol. Biol.* **2004**, *343*, 1019–1030.

[3] U. Eder, G. Sauer, R. Wiechert, *Angew. Chem. Int. Ed. Engl.* **1971**, *10*, 496–497; *Angew. Chem.* **1971**, *83*, 492–493.

[4] a) Z. G. Hajos, D. R. Parrish, *German Patent* DE2120623; b) Z. G. Hajos, D. R. Parrish, *J. Org. Chem.* **1974**, *39*, 1615–1621.

[5] a) B. List, R. A. Lerner, C. F. Barbas III, *J. Am. Chem. Soc.* **2000**, *122*, 2395–2396; b) For the extension to an L-Pro-catalyzed Robinson reaction, see: T. Bui, C. F. Barbas III, *Tetrahedron Lett.* **2000**, *41*, 6951–6954; c) See also: C. F. Barbas III, *Angew. Chem. Int. Ed.* **2008**, *47*, 42–47; *Angew. Chem.* **2008**, *120*, 46–51.

[6] B. List, P. Pojarliev, C. Castello, *Org. Lett.* **2001**, *3*, 573–575.

[7] a) W. Notz, F. Tanaka, C. F. Barbas III, *Acc. Chem. Res.* **2004**, *37*, 580–591; b) B. List, J. W. Yang, *Science* **2006**, *313*, 1584–1586; c) S. Mukherjee, J. W. Yang, S. Hoffmann, B. List, *Chem. Rev.* **2007**, *107*, 5471–5569; d) G. Guillena, C. Nájera, D. J. Ramón, *Tetrahedron: Asymmetry* **2007**, *18*, 2249–2293; e) M. J. Gaunt, C. C. C. Johansson, A. McNally, N. T. Vo, *Drug Discovery Today* **2007**, *12*, 8–27; f) A. Dondoni, A. Massi, *Angew. Chem. Int. Ed.* **2008**, *47*, 4638–4660; *Angew. Chem.* **2008**, *120*, 4718–4742; P. Melchiorre, M. Marigo, A. Carlone, G. Bartoli, *Angew. Chem. Int. Ed.* **2008**, *47*, 6138–6171; *Angew. Chem.* **2008**, *120*, 6232–6265; S. Bertelsen, K. A. Jørgensen, *Chem. Soc. Rev.* **2009**, *38*, 2178–2189; i) M. Nielsen, D. Worgull, T. Zweifel, B. Gschwend, S. Bertelsen, K. A. Jørgensen, *Chem. Commun.* **2010**, *46*, 632–649; j) J. G. Hernández, E. Juaristi, *Chem. Commun.* **2012**, *48*, 5396–5409.

[8] a) K. A. Ahrendt, C. J. Borths, D. W. C. MacMillan, *J. Am. Chem. Soc.* **2000**, *122*, 4243–4244; b) D. W. C. MacMillan, *Nature* **2008**, *455*, 304–308.

[9] a) S. G. Zlotin, A. S. Kucherenko, I. P. Beletskaya, *Russ. Chem. Rev.* **2009**, *78*, 737–784; b) H. Wennemers, *Chimia* **2010**, *64*, 864–865; c) U. Scheffer, R. Mahrwald, *Synlett* **2011**, 1660–1667; d) V. Bisai, A. Bisai, V. K. Singh, *Tetrahedron* **2012**, *68*, 4541–4580.

[10] a) Y. Hayashi, T. Itoh, N. Nagae, M. Ohkubo, H. Ishikawa, *Synlett* **2008**, 1565–1570; b) M. Amedjkouh, *Tetrahedron: Asymmetry* **2007**, *18*, 390–395; c) M. Majewski, I. Niewczas, N. Palyam, *Synlett* **2006**, 2387–2390; d) A. Córdova, W. Zou, P. Dziedzic, I. Ibrahem, E. Reyes, Y. Xu, *Chem. Eur. J.* **2006**, *12*, 5383–5397.

[11] a) Y. Lam, K. N. Houk, U. Scheffler, R. Mahrwald, *J. Am. Chem. Soc.* **2012**, *134*, 6286–6295; b) M. Markert, U. Scheffler, R. Mahrwald, *J. Am. Chem. Soc.* **2009**, *131*, 16642–16643; c) U. Scheffler, R. Mahrwald, *J. Org. Chem.* **2012**, *77*, 2310–2330.

[12] S. S. V. Ramasastry, H. Zhang, F. Tanaka, C. F. Barbas III, *J. Am. Chem. Soc.* **2007**, *129*, 288–289.

[13] S. S. V. Ramasastry, K. Albertshofer, N. Utsumi, C. F. Barbas III, *Org. Lett.* **2008**, *10*, 1621–1624.

[14] a) S. S. V. Ramasastry, K. Albertshofer, N. Utsumi, F. Tanaka, C. F. Barbas III, *Angew. Chem. Int. Ed.* **2007**, *46*, 5572–5575; *Angew. Chem.* **2007**, *119*, 56[illegible]) Z. Jiang, H. Yang, X. Han, J. Luo, M. W. Wong, Y. Lu, *Org. Biomol. Chem.* **2010**, *8*, 1368–1377.

[15] A. Bassan, W. Zou, E. Reyes, F. Himo, A. Córdova, *Angew. Chem. Int. Ed.* **2005**, *44*, 7028–7032; *Angew. Chem.* **2005**, *117*, 719[illegible]

[16] K. Rohr, R. Mahrwald, *Org. Lett.* **2012**, *14*, 2180–2183.

[17] B. M. Trost, C. S. Brindle, *Chem. Soc. Rev.* **2010**, *39*, 1600–1632.

[18] a) B. List, L. Hoang, H. J. Martin, *Proc. Natl. Acad. Sci. USA* **2004**, *101*, 5839–5842; b) M. B. Schmid, K. Zeitler, R. M. Gschwind, *Angew. Chem. Int. Ed.* **2010**, *49*, 4997–5003; *Angew. Chem.* **2010**, *122*, 51[illegible] H. Zhu, F. R. Clemente, K. N. Houk, M. P. Meyer, *J. Am. Chem. Soc.* **2009**, *131*, 1632–1633; d) D. Seebach, A. K. Beck, D. M. Badine, M. Limbach, A. Eschenmoser, A. M. Treasurywala, R. Hobi, W. Prikoszovich, B. Linder, *Helv. Chim. Acta* **2007**, *90*, 425–471.

[19] a) P. H.-Y. Cheong, C. Legaut, J. M. Um, N. Çelebi-Ölçum, K. N. Houk, *Chem. Rev.* **2011**, *111*, 5042–5137; b) A. K. Sharma, R. B. Sunoj, *Angew. Chem. Int. Ed.* **2010**, *49*, 6373–6377; *Angew. Chem.* **2010**, *122*, 65[illegible] M. P. Patil, R. B. Sunoj, *J. Org. Chem.* **2007**, *72*, 8202–8215; d) F. R. Clemente, K. N. Houk, *J. Am. Chem. Soc.* **2005**, *127*, 11294–11302; e) C. Allemann, R. Gordillo, F. R. Clemente, P. H.-Y. Cheong, K. N. Houk, *Acc. Chem. Res.* **2004**, *37*, 558–569; f) F. R. Clemente, K. N. Houk, *Angew. Chem. Int. Ed.* **2004**, *43*, 5766–5768; *Angew. Chem.* **2004**, *116*, 589[illegible] S. Bahmanyar, K. N. Houk, *Org. Lett.* **2003**, *5*, 1249–1251; h) L. Hoang, S. Bahmanyar, K. N. Houk, B. List, *J. Am. Chem. Soc.* **2003**, *125*, 16–17; i) K. N. Rankin, J. W. Gauld, R. J. Boyd, *J. Phys. Chem. A* **2002**, *106*, 5155–5159.

[20] In the absence of acidic protons in the reaction media, L-proline methyl ester yields racemic aldol adducts, see: A. Bøgevic, N. Kumaragurubaran, K. A. Jørgensen, *Chem. Commun.* **2002**, 620–621.

[21] a) M. B. Schmid, K. Zeitler, R. M. Gschwind, *J. Org. Chem.* **2011**, *76*, 3005–3015; b) C. Marquez, J. O. Metzger, *Chem. Commun.* **2006**, 1539–1541.

[22] D. A. Bock, C. W. Lehman, B. List, *Proc. Natl. Acad. Sci. USA* **2010**, *107*, 20636–20641.

[23] S. Bahmanyar, K. N. Houk, H. J. Martin, B. List, *J. Am. Chem. Soc.* **2003**, *125*, 2475–2479.

[24] H. E. Zimmerman, M. D. Traxler, *J. Am. Chem. Soc.* **1957**, *79*, 1920–1923.

[25] a) A. de Cózar, F. P. Cossío, *Phys. Chem. Chem. Phys.* **2011**, *13*, 10858–10868; b) C. Nájera, J. M. Sansano, *Chem. Rev.* **2007**, *107*, 4584–4671; c) G. Pandeym, P. Banerjee, S. R. Gadre, *Chem. Rev.* **2006**, *106*, 4484–4517; d) C. Nájera, J. M. Sansano, *Angew. Chem. Int. Ed.* **2005**, *44*, 6272–6276; *Angew. Chem.* **2005**, *117*, 6428; e) C. Nájera, M. G. Retamosa, J. M. Sansano, *Angew. Chem. Int. Ed.* **2008**, *47*, 6055–6058; *Angew. Chem.* **2008**, *120*, 614[illegible]

[26] E. Conde, D. Bello, A. de Cózar, M. Sánchez, M. A. Vázquez, F. P. Cossío, *Chem. Sci.* **2012**, *3*, 1486–1491.

[27] L. M. Castelló, C. Nájera, J. M. Sansano, O. Larrañaga, A. de Cózar, F. P. Cossío, *Org. Lett.* **2013**, *15*, 2902–2905.

[28] a) A. Arrieta, D. Otaegui, A. Zubia, F. P. Cossío, A. Díaz-Ortiz, A. de la Hoz, M. A. Herrero, P. Prieto, C. Foces-Foces, J. L. Pizarro, M. I. Arriortua, *J. Org. Chem.* **2007**, *72*, 4313–4322; b) S. Vivanco, B. Lecea, A. Arrieta, P. Prieto, I. Morao, A. Linden, F. P. Cossío, *J. Am. Chem. Soc.* **2000**, *122*, 6078–6092; c) M. Ayerbe, A. Arrieta, F. P. Cossío, A. Linden, *J. Org. Chem.* **1998**, *63*, 1795–1825.

[29] CCDC-965082 (for *exo′*-L-**10aa**) contains the supplementary crystallographic data for this paper. These data can be obtained free of charge from The Cambridge Crystallographic Data Centre via www.ccdc.cam.ac.uk/data_request/cif. The absolute configuration of *exo′*-L-**10aa** was unambiguously assigned by considering the Flack parameter value: 0.008(6); see the Supporting Information for details.

[30] E. V. Anslyn, D. A. Dougherty, *Modern Physical Organic Chemistry*, University Science Books, Sausalito, CA, **2006**, p. 507–523.

[31] H. Lineweaver, D. Burk, *J. Am. Chem. Soc.* **1934**, *56*, 658–666.

[32] C. J. Rogers, T. J. Dickerson, K. D. Janda, *Tetrahedron* **2006**, *62*, 352–356.

[33] N. Zotova, L. J. Broadbelt, A. Armstrong, D. G. Blackmond, *Bioorg. Med. Chem. Lett.* **2009**, *19*, 3934–3937.

[34] D. C. Harris, *Experimental Error in Quantitative Chemical Analysis*, 8th ed., W. H. Freeman, New York, **2010**, p. 51–67.

[35] N. L. L. Allinger, *Molecular Structure. Understanding Steric and Electronic Effects from Molecular Mechanics*, Wiley, Hoboken, N.J. **2010**.

[36] a) *MacroModel*, version 9.9, Schrodinger LLC, New York, NY, **2012**; b) F. Mohamadi, N. G. J. Richards, W. C. Guida, R. Liskamp, M. Lipton, C. Caulfield, G. Chang, T. Hendrickson, W. C. Still, *J. Comput. Chem.* **1990**, *11*, 440–467.

[37] J. P. Rickaert, G. Ciccotti, H. J. C. Berendsen, *J. Comp. Physiol.* **1977**, *23*, 327–341.

[38] M. J. Frisch, G. W. Trucks, H. B. Schlegel, G. E. Scuseria, M. A. Robb, J. R. Cheeseman, G. Scalmani, V. Barone, B. Mennucci, G. A. Petersson, H. Nakatsuji, M. Caricato, X. Li, H. P. Hratchian, A. F. Izmaylov, J. Bloino, G. Zheng, J. L. Sonnenberg, M. Hada, M. Ehara, K. Toyota, R. Fukuda, J. Hasegawa, M. Ishida, T. Nakajima, Y. Honda, O. Kitao, H. Nakai, T. Vreven, J. A. Montgomery Jr., J. E. Peralta, F. Ogliaro, M. Bearpark, J. J. Heyd, E. Brothers, K. N. Kudin, V. N. Staroverov, R. Kobayashi, J. Normand, K. Raghavachari, A. Rendell, J. C. Burant, S. S. Iyengar, J. Tomasi, M. Cossi, N. Rega, J. M. Millam, M. Klene, J. E. Knox, J. B. Cross, V. Bakken, C. Adamo, J. Jaramillo, R. Gomperts, R. E. Stratmann, O. Yazyev, A. J. Austin, R. Cammi, C. Pomelli, J. W. Ochterski, R. L. Martin, K. Morokuma, V. G. Zakrzewski, G. A. Voth, P. Salvador, J. J. Dannenberg, S. Dapprich, A. D. Daniels, O. Farkas, J. B. Foresman, J. V. Ortiz, J. Cioslowski, D. J. Fox, *Gaussian 09*, revision B.01, Gaussian, Inc., Wallingford CT, **2009**.

[39] a) C. Lee, W. Yang, R. G. Parr, *Phys. Rev. B* **1988**, *37*, 785–789; b) A. D. Becke, *J. Chem. Phys.* **1993**, *98*, 1372–1377; c) A. D. Becke, *J. Chem. Phys.* **1993**, *98*, 5648–5652.

[40] a) R. Cammi, B. Mennucci, J. Tomasi, *J. Phys. Chem. A* **2000**, *104*, 5631–5637; b) J. Tomasi, B. Mennucci, R. Cammi, *Chem. Rev.* **2005**, *105*, 2999–3093.

[41] a) Y. Zhao, D. G. Truhlar, *J. Chem. Theory Comput.* **2008**, *4*, 1849–1868; b) Y. Zhao, D. G. Truhlar, *Acc. Chem. Res.* **2008**, *41*, 157–167; c) Y. Zhao, D. G. Truhlar, *Theor. Chem. Acc.* **2008**, *120*, 215–241.

Received: February 2, 2015

EurJOC European Journal of Organic Chemistry

Densely substituted enantiopure proline esters obtained through [3+2] cycloadditions catalyze aldol reactions. These synthetic organocatalysts produce different enantiomeric aldol adducts depending on the stereochemical dispositions of the substituents at distal positions with respect to the catalytic site. Design criteria are proposed for this kind of organocatalysts.

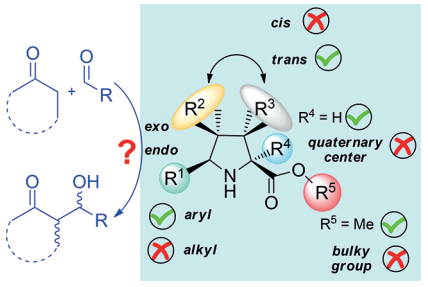

Keywords: Organocatalysis / Aldol reactions / Kinetics / Reaction mechanisms / Transition states

